A critical analysis of drag force modelling for disperse gas-liquid flow in a pipe with an obstacle

Tas-Köhler, S.; Liao, Y.; Hampel, U.;

Originally published:

August 2021

Chemical Engineering Science 246(2021), 117007

DOI: https://doi.org/10.1016/j.ces.2021.117007

Chemical Engineering Science

A critical analysis of drag force modelling for disperse gas-liquid flow in a pipe with an obstacle

--Manuscript Draft--

Manuscript Number:	
Article Type:	Research paper
Section/Category:	Transport Phenomena, including Fluid Mechanics
Keywords:	CFD; bubbly flow; drag force coefficient; turbulence; vortex; hybrid drag model
Corresponding Author:	Sibel Tas-Koehler, M. Sc. Helmholtz-Zentrum Dresden-Rossendorf Dresden, Sachsen GERMANY
First Author:	Sibel Tas-Koehler, M. Sc.
Order of Authors:	Sibel Tas-Koehler, M. Sc.
	Yixiang Liao
	Uwe Hampel
Abstract:	The accuracy of gas-liquid flow modelling depends on an appropriate modelling of interfacial forces. Among those, the drag is dominating. Most drag models have been derived and validated for laminar or low-turbulence flow conditions only. In this study, we evaluated different drag models from the literature for a highly turbulent gas-liquid flow around an obstacle in a pipe that produces a pronounced vortex region. We compared void fraction, as well as gas and liquid velocity profiles with experimental data obtained by means of Ultrafast X-ray Computed Tomography. We found that all the models except Bakker and Feng, predict the void fraction well compared to experimental data upstream of the obstacle, that is, for a developed two-phase pipe flow with axial symmetry. However, the void fraction downstream is grossly overestimated by all of the models. Based on the results, a hybrid drag model is proposed, which improves void fraction predictions considerably.
Suggested Reviewers:	Ning Yang nyang@ipe.ac.cn
	Mohsen Karimi karimi@sun.ac.za
	Amjad Asad Amjad.Asad@imfd.tu-freiberg.de
	Jyeshtharaj Joshi jbj@udct.org
	Milton Mori mori@feq.unicamp.br
	Shantanu Roy roys@chemical.iitd.ac.in
Opposed Reviewers:	

Highlights

- The capability of different drag models under high turbulence /vortex flow conditions is shown.
- Impacts of turbulence effects on drag modelling is presented.
- A hybrid model is proposed for high turbulence flow conditions.
- Two-phase flow hydrodynamics under complex flow conditions is analyzed.
- Phase velocities and void fraction predictions are compared with experimental data

A critical analysis of drag force modelling for disperse gas-liquid flow in a pipe with an obstacle

Sibel Tas-Koehler [a]*, Yixiang Liao [a], Uwe Hampel [a,b]

[a] Helmholtz-Zentrum Dresden-Rossendorf, Institute of Fluid Dynamics, Bautzner Landstr. 400, 01328 Dresden, Germany

[b] Technische Universität Dresden, Chair of Imaging Techniques in Energy and Process Engineering, 01062 Dresden, Germany

* Corresponding author (E-mail: s.tas@hzdr.de)

ABSTRACT

The accuracy of gas-liquid flow modelling strongly depends on an appropriate modelling of interfacial forces. Among those, the drag is dominating. Most drag models reported in the literature have been derived and validated for laminar or low-turbulence flow conditions only. In this study, we evaluated different drag models from the literature for a highly turbulent gas-liquid flow around an obstacle in a pipe that produces a pronounced vortex region. We compared void fraction, as well as gas and liquid velocity profiles with experimental data obtained by means of Ultrafast X-ray Computed Tomography. We found that all the models except Bakker and Feng, predict the void fraction well compared to experimental data upstream of the obstacle, that is, for a developed two-phase pipe flow with axial symmetry. However, the void fraction downstream is grossly overestimated by all of the models. Based on the results, a hybrid drag model is proposed, which improves void fraction predictions considerably.

Keywords: CFD, bubbly flow, drag force coefficient, turbulence, vortex, hybrid drag model

Nomenclature

Latin symbols		**Greek symbols**	
d_B	bubble diameter [m]	α	gas volume fraction [-]
C_D	drag coefficient [-]	ν	kinematic viscosity [$m^2 \cdot s^{-1}$]
Eo	Eötvös number [-]	σ	surface tension [$kg \cdot s^{-2}$]
F_D	drag force per unit volume [$N \cdot m^{-3}$]	ε	turbulence dissipation rate [$m^2 \cdot s^{-3}$]
k	phase indicator	μ	dynamic viscosity [$kg \cdot m^{-1} \cdot s^{-1}$]
M_i	source term in i-th direction [$kg \cdot m^{-2} \cdot s^{-2}$]	$\tau_{ij}^{Lam}, \tau_{ij}^{Turb}$	laminar stress tensor [$kg \cdot m^{-1} \cdot s^{-2}$], turbulent stress tensor [$kg \cdot m^{-1} \cdot s^{-2}$]
Mo	Morton number [-]	ρ	density [$kg \cdot m^{-3}$]
p	pressure [Pa]	**Subscripts**	

Re	Reynolds number [-]	B	bubble
u	velocity [m·s^{-1}]	L	liquid phase
		G	gas phase

Acronyms

BIT: Bubble-Induced Turbulence
CFD: Computational Fluid Dynamics
FAD: Favre-Averaged Drag
MUSIG: Multiple Size Group Model
SST: Shear Stress Transport
UFXCT: Ultrafast X-ray Computed Tomography

1. Introduction

Bubbly flows are important in many fields of process, energy and environmental engineering. Examples are boiling two-phase flow in nuclear reactors (Tas-Koehler *et al.* (2020)), stirred tanks (Guan *et al.* (2020)), bubble columns (Besagni *et al.* (2018)) and airlift reactors (Jiang *et al.* (2016)). In all these applications the modelling and simulation of two-phase flow is required to understand and predict heat and mass transfer, mixing efficiency and chemical reaction (Guan *et al.* (2020); Pourtousi *et al.* (2014)). Computational fluid dynamics (CFD) has meanwhile considerably progressed to simulate two-phase flows. However, there are still major challenges with complex three-dimensional flow situations. One example is two-phase flow near impeller blades in reactors where gas accumulates in local vortex regions. Another example is flow separation behind spacers with vanes in nuclear fuel assemblies. Yet, a third example is bubble columns with internals. For all these applications, improved numerical CFD modelling is needed. Especially for the Euler-Euler CFD modelling context this requires appropriate closure equations for interfacial forces (Liao *et al.* (2018)).

In two-phase bubbly flow simulations, the momentum exchange between the phases is calculated via interfacial forces such as drag, lift, turbulent dispersion, wall lubrication and virtual mass. Among them, the drag force is the dominant force with a significantly higher magnitude than the other forces. Hence, accurate drag modelling is of primary importance (Chen (2004); Pourtousi *et al.* (2014); Yamoah *et al.* (2015)).

The interfacial drag force

$$\boldsymbol{F}_D = -\frac{3}{4}\frac{C_D}{d_B}\alpha\rho_L|\boldsymbol{u}_G - \boldsymbol{u}_L|\,(\boldsymbol{u}_G - \boldsymbol{u}_L) \tag{1}$$

determines the relative velocity between two phases as well as lateral migration of the gas phase. Here, d_B is the bubble diameter, α is the gas void fraction, ρ_L is the liquid density, $\boldsymbol{u}_G$ is the gas velocity, $\boldsymbol{u}_L$ is the liquid velocity and C_D is the drag coefficient. A large number of C_D closures have been proposed for the drag model in the literature. Most of the closures were obtained from bubble rise in stagnant liquid experiments. Schiller & Naumann (1935) developed a C_D model by considering a single and rigid sphere bubble for a wide range of Re_B

$$Re_B = \frac{\rho_L|\boldsymbol{u}_L - \boldsymbol{u}_G|d_B}{\mu_L}. \tag{2}$$

The Schiller&Naumann model gives good results for the small spherical bubbles (up to a diameter of 2.5 mm) and the low void fraction cases. However, it does not consider the deformation of the bubbles.

In addition, this model uses a constant C_D for high Re_B. Morsi & Alexander (1972) correlated a C_D model for a wide range of Re_B. However, the model includes different constants for different ranges of Re_B. Grace *et al.* (1976) improved the Schiller&Naumann model by considering the bubble deformation. The Grace model bases three non-dimensional numbers: Re_B, Eötvös number (Eo)

$$Eo = \frac{g(\rho_L - \rho_G){d_B}^2}{\sigma} \tag{3}$$

and Morton number (Mo)

$$Mo = \frac{g(\rho_L - \rho_G)\mu_L^4}{{\rho_L}^2\sigma^3}. \tag{4}$$

Similar to the Schiller&Naumann model, the Grace model is suitable for low void fraction cases. Ishii & Zuber (1979) developed C_D correlations for bubbly flow by considering also the bubble deformation. They compared the drag coefficients with experimental data and obtained satisfactory agreements in a wide range of the particle concentration and Reynolds number. Although the application range was not given explicitly, it is expected to be valid approximately for $Eo < 10^6$ and $Re_B < 10^4$ (Asad *et al.* (2017)). The main difference between the Ishii&Zuber and the Grace model is the definition of C_D for ellipsoidal bubbles ($C_{Dellipse}$). Silva et al. (2012) investigated the capability of the Ishii&Zuber model for the heterogeneous flow in a bubble column. They found that the Ishii&Zuber model overestimates the gas holdup compared to experimental data. Masood & Delgado (2014) compared the above drag models (Ishii&Zuber, Grace and Schiller&Naumann) and showed that while all drag models provide reasonable liquid axial velocity results compared to experiments, the model of Ishii&Zuber predicts axial gas velocity better than the other two models.

Tomiyama et al. (1998) developed C_D closures from experimental data of a single bubble in a stagnant liquid that include the effects of not only fluid properties, gravity, bubble deformation but also the degree of contamination (pure, moderately contaminated and fully contaminated). The correlations depend on two non-dimensional numbers, i.e. Re_B and Eo. They are valid for $10^{-2} < Eo < 10^3$ and $10^{-3} < Re_B < 10^5$. Zhang & VanderHeyden (2002) developed a C_D model, which is a function of Re_B only. The range of applicability for Zhang&VanderHeyden model was not given explicitly. Simonnet et al. (2007) empirically derived a C_D model without bubble deformation and Re_B consideration, yet, the model includes a correction factor that is account for the influence of local void fraction. Since the Tomiyama model considers different flow properties and is applicable for high Re_B cases, it has often been compared with other models in the literature, especially for bubble columns. Zhang *et al.* (2006) compared Ishii&Zuber and Tomiyama drag models for two different square-cross sectioned bubble columns of two different aspect ratios. They found that with the Tomiyama model, the predicted slip velocity agrees well with the experimental data in both columns. Besagni et al. (2018) compared the Tomiyama and Grace models for small-scale and large-scale bubble columns. They found that the Tomiyama model provides a better agreement to experimental data in terms of a void fraction. Tabib et al. (2008) compared the Schiller&Naumann, Ishii&Zuber, the Grace and Zhang&VanderHeyden models to estimate the gas-liquid flow pattern in bubble columns. The results showed that whereas the predictions of the Ishii&Zuber and Zhang&VanderHeyden models are closer to experimental data for low superficial gas velocity, only the Zhang&VanderHeyden model is appropriate for predicting the flow pattern at high superficial gas velocity. Gupta & Roy (2013) investigated four drag models e.g. Schiller&Naumann, Tomiyama, Ishii&Zuber and Zhang&VanderHeyden to study gas-liquid in a bubble column. They found that all drag models provide similar axial liquid velocity predictions for low gas holdup and superficial velocities. However, they underlined that further studies are necessary for higher gas velocities. Jin et al. (2019) compared the drag models of Ishii&Zuber, Tomiyama, Simonnet and Grace. They reported that Tomiyama gives better void fraction results compared to the experimental data for medium to high Re_B number and low void fraction. Wang & Yao (2016) analysed different interface force models for gas-liquid flow and found that for the low bubble Reynolds number (Re_B), Schiller&Naumann, Morsi&Alexander, Grace, Tomiyama and Ishii&Zuber models provide similar results in terms of radial void fraction. However, for the high Re_B, only Grace, Tomiyama and Ishii&Zuber models, which consider bubble deformation, showed good accuracy. Yamoah et al. (2015) numerically investigated different drag models such as Grace, Ishii&Zuber, Tomiyama and Simonnet. All drag coefficient correlations provided satisfying void fraction results in comparison with experimental data. Although the Tomiyama model provides good predictions for both bubble column and pipe geometry, it is not the case for an external loop reactor, which has more flow complexity. Jiang *et al.* (2016) investigated the performance of Tomiyama, Schiller&Naumann and dual bubble size (DBS)-local model for an external loop airlift reactor. They found that the Schiller&Naumann model underestimates the local gas holdup at lower superficial gas velocity whereas the Tomiyama model overestimates it at higher superficial gas velocity.

In a turbulent flow, a bubble undergoes continuous acceleration and deceleration as well as deformation due to turbulent eddies. The impact of turbulent eddies on the motion of the gas phase is generally ignored by assuming a standard drag model that has been obtained in quiescent flow. Such an assumption can cause considerable errors in the void fraction profile under turbulent conditions (Doroodchi *et al.* (2008)). Thus, there are drag closures that consider turbulence effects in the literature. Bakker & Vandenakker (1994) attempted to describe the effect of turbulence on the drag coefficient by utilizing a modified Reynolds number in a common correlation developed for stagnant fluid. Brucato *et al.* (1998) performed experiments to measure drag coefficients of solid particles in a turbulent flow. They proposed a new drag coefficient correlation based on the Tomiyama model by considering the ratio of bubble diameter to the Kolmogorov length scale (based on volume-averaged energy dissipation rate) of turbulence. Lane *et al.* (2002) applied the Brucato model to bubbles since the mechanism of drag modification is believed to be similar and confirmed that the Brucato model can be used for the bubbles. Lane *et al.* (2005) proposed a C_D model that is based on the available experimental data in the literature. They found that there is a relation between the ratio of the slip velocity to the particle terminal velocity and drag coefficient.

Khopkar & Ranade (2006) compared the drag models of Brucato and Bakker for a stirred vessel. They showed that the Brucato model provides better agreement with the experimental data for the gas holdup. Karimi *et al.* (2012) numerically investigated the performance of Schiller&Naumann and Lane drag models in a Rushton-turbine flotation tank under turbulent conditions. They found that while the Schiller&Naumann model overestimate the gas holdup compared to experimental data, the Lane model provides fair agreement. Feng & Bolotnov (2016) proposed a modified version of Tomiyama model for C_D based on DNS simulations. However, the model does not consider the bubble deformation. They indicated that the modified model is valid for Re_B up to 900. Thus, they point out that further investigations are needed to validate its applicability on higher Re_B. Salibindla et al. (2020) calculated C_D of deforming bubbles in isotropic turbulence at a high-energy dissipation rate ($\varepsilon \sim 0.5\ m^2 s^{-3}$) via measurements of mean bubble and flow vertical velocity. They showed that when $Re_B < 400$, the results agree well with the data of the Tomiyama model for bubbles rising in contaminated water. For $Re_B > 400$, they developed a new C_D model based on a turbulence-based Weber number. Mathematical descriptions of all aforementioned models are given in Table 1.

The literature review shows that whereas the Schiller&Naumann model predicts axial gas and liquid velocities satisfactorily, yet, it underestimates the local void fraction at low superficial gas velocity, the Ishii&Zuber model predicts axial gas and liquid velocities well for low void fraction and superficial velocities, yet, it overestimates the void fraction. The Tomiyama model generally provides good void fraction accuracy for medium to high Re_B number and low void fraction. However, when there is flow complexity, the Tomiyama model overestimates the void fraction. The Brucato model predicts the void fraction well at high turbulence. For the Feng and Salibindla models, investigations are still required. It can be concluded that it is not clear whether available drag models are appropriate for complex two-phase flow simulations. In addition, the available drag models, which are appropriate for high turbulence, also need validation in the presence of a vortex region where sudden shear changes are present. In this context, the aim of the study, to evaluate the capability of drag models under the high turbulence-uniform/vortex flow conditions that have a more practical use for engineering applications. Thus, a capability analysis of the different drag models in the Euler-Euler framework of bubbly flow simulations was performed for the case of a half-obstructed pipe and two different turbulence conditions. Both the capability of the most widely applied C_D models in the literature for low- and high-turbulence conditions (i.e. Schiller&Naumann, Grace, Ishii&Zuber, Tomiyama) and less applied C_D models that consider the turbulence effects (i.e. Bakker, Brucato, Feng and Salibindla) were investigated. Simulated gas volume fraction, liquid velocity and gas velocity are compared against experimental data of Neumann-Kipping *et al.* (2020).

Table 1: Summary of the drag closure models considered in the literature review.

Reference	Mathematical description
Schiller&Naumann model	$C_D = \begin{cases} 24\left(1+0.15{Re_B}^{0.687}\right)/Re_B & Re_B \leq 1000 \\ 0.44 & Re_B > 1000 \end{cases}$
Morsi&Alexander model	$C_D = a_1 + \frac{a_2}{Re_B} + \frac{a_3}{Re_B} \qquad a_1, a_2, a_3 = \begin{cases} 0, 24, 0 & 0 < Re_B < 0.1 \\ 3.69, 22.73, 0.0903 & 0.1 < Re_B < 1 \\ 1.222, 29.1667, -3.8889 & 1 < Re_B < 10 \\ 0.6167, 46.50, -116.67 & 10 < Re_B < 100 \\ 0.3644, 98.33, -2778 & 100 < Re_B < 1000 \\ 0.357, 148.62, -47500 & 1000 < Re_B < 5000 \\ 0.46, -490.546, 578700 & 5000 < Re_B < 10000 \\ 0.5191, -1662.5, 5416700 & Re_B \geq 10000 \end{cases}$
Grace model	$C_D = max\left[C_{Dsphere}, min\left(C_{Dellipse,}, C_{Dcap}\right)\right]$ $C_{Dsphere} = \begin{cases} \dfrac{24}{Re_B} & Re_B \leq 0.01 \\ \max\left(\dfrac{24}{Re_B}\left(1+0.15{Re_B}^{0.687}\right), 0.44\right) & 0.01 > Re_B \end{cases} \quad C_{Dcap} = \frac{8}{3}, \quad C_{Dellipse} = \frac{4}{3}\frac{g d_B}{U_t^2}\frac{(\rho_L - \rho_G)}{\rho_L},$ $U_t = \frac{\mu_L}{d_B \rho_L} Mo^{-0.149}(J - 0.857), \quad J = \begin{cases} 0.94H^{0.757} & 2 < H \leq 59.3 \\ 3.42H^{0.441} & H > 59.3 \end{cases}, \quad H = \frac{4}{3} Eo Mo^{-0.149}\left(\frac{\mu_L}{9x10^{-4}}\right)^{-0.14}$
Ishii&Zuber model	$C_D = max\left[C_{Dsphere}, min\left(C_{Dellipse,}, C_{Dcap}\right)\right]$ *spherical regime* $0 \leq Re_B < 1000$, *ellipse and cap regime* $Re_B > 1000$ $C_{Dsphere} = \frac{24}{Re_B}\left(1 + 0.1{Re_B}^{3/4}\right), \quad C_{Dellipse} = \frac{2}{3}\sqrt{Eo}, \quad C_{Dcap} = \frac{8}{3}$
Bakker model	$C_D = \frac{24}{Re_B^*}\left(1 + 0.15{Re_B}^{0.687}\right), \ Re_B^* = \frac{\rho_L \lvert \boldsymbol{u}_L - \boldsymbol{u}_G \rvert d_B}{\mu_L + \frac{2}{9}\mu_t}$

Tomiyama model	$C_D = max\left[min\left(\frac{16}{Re_B}\left(1+0.15{Re_B}^{0.687}\right), \frac{48}{Re_B}\right), \frac{8Eo}{3(Eo+4)}\right]\ (pure)$ $C_D = max\left[min\left(\frac{24}{Re_B}\left(1+0.15{Re_B}^{0.687}\right), \frac{72}{Re_B}\right), \frac{8Eo}{3(Eo+4)}\right]\ (moderately\ conttaminated)$ $C_D = max\left[\left(\frac{24}{Re_B}\left(1+0.15{Re_B}^{0.687}\right)\right), \frac{8Eo}{3(Eo+4)}\right]\ (fully\ contaminated)$
Brucato model	$\frac{C_D - C_{D0}}{C_{D0}} = 6.5\times 10^{-6}\left(\frac{d_B}{\lambda}\right)^3, \quad \lambda = \left(\frac{\nu^3}{\varepsilon}\right)^{1/4} \quad C_{D0} = max\left[\left(\frac{24}{Re_B}\left(1+0.15{Re_B}^{0.687}\right)\right), \frac{8Eo}{3(Eo+4)}\right]$
Zhang&VanderHeyden model	$C_D = 0.44 + \frac{24}{Re_B} + \frac{6}{1+\sqrt{Re_B}}$
Lane model	$\frac{C_D}{C_{D0}} = \left(\frac{U_S}{U_T}\right)^{-2}, \ \frac{U_S}{U_T} = 1 - 1.4\left(\frac{\tau_B}{T_L}\right)^{0.7} exp\left(-0.6\left(\frac{\tau_B}{T_L}\right)\right), \ \tau_B = \frac{U_T}{2g}, \quad T_L = 0.135\frac{k}{\varepsilon}$
Simonnet model	$C_D = C_{D\infty}E_\infty, \quad C_{D\infty} = \frac{4}{3}\frac{\rho_L-\rho_G}{\rho_L} g d_B \frac{1}{U_t^2}, \quad U_t = \frac{u_{b1}u_{b2}}{\sqrt{{u_{b1}}^2+{u_{b2}}^2}}, \quad u_{b1} = \frac{1}{18}\frac{\rho_L-\rho_G}{\mu_L} g {d_B}^2\left(\frac{3\mu_G+3\mu_L}{3\mu_G+2\mu_L}\right),$ $u_{b2} = \sqrt{\frac{2\sigma}{(\rho_L-\rho_G)d_B} + \frac{g d_B}{2}}, \quad E_\infty = (1-\alpha_G)\left[(1-\alpha_G)^m + \left(4.8\frac{\alpha_G}{1-\alpha_G}\right)^m\right]^{-2/m}, \ m = 25$
Feng model	$C_D = \min\left[\frac{16}{Re_b}\left(1+0.15{Re_B}^{0.687}\right), \frac{48}{Re_B}\left(1+3x10^{-10}{Re_B}^{3.3189}\right)\right]$
Salibindla model	$C_D = max\left(\frac{24}{Re_B}\left(1+0.15{Re_B}^{0.687}\right), min\left(f(Eo), f(Eo)/We^{1/3}\right)\right), \ f(Eo) = \frac{8Eo}{3(Eo+4)}, We = 2.13\rho(\varepsilon d_B)^{2/3} d_B/\sigma$

2. Experimental setup

Numerical results were compared against experimental data of Neumann-Kipping *et al.* (2020). The experiments were carried out at a vertical pipe of 4950 mm height and 54 mm inner diameter (Fig.1). A semi-circular obstacle that blocks half of the inner pipe cross-section was used to generate a vortex region. During the experiment, water was circulated upwards through the pipe and air was injected via a gas injection module from the bottom of the pipe at 4 bar and 30°C. Two test cases with different liquid velocities are considered (Table 2).

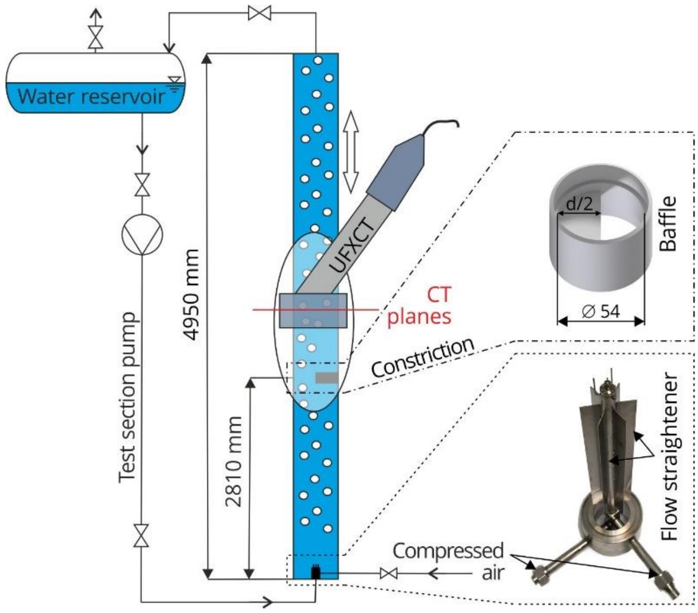

Figure 1: Schematic representations of the vertical test section (left) with details of the gas injection module (bottom right) and the flow obstacle for generation of three-dimensional flow fields (top right) (Tas-Koehler et al. (2021)).

Table 2: Experimental operating conditions based on combinations of liquid and gas superficial velocities.

Test case	j_l [m·s^{-1}]	j_g [m·s^{-1}]
072	0.4050	0.0368
074	1.0170	0.0368

Ultrafast X-ray computed tomography (UFXCT) was applied to obtain the local gas and liquid distribution. This technique provides detailed data on the flow structure with a high resolution in space and time. For details on the experiments and data evaluation, the interested reader is referred to Neumann-Kipping et al. (2020) and Tas-Koehler et al. (2021).

3. Numerical setup

In the present work, the same numerical setup as already reported in Tas-Koehler *et al.* (2021) was used. 3D steady state simulations with an Eulerian-Eulerian two-fluid model were carried out using ANSYS CFX 19.2. The fluid domain was modelled from 1.5 m upstream to 1 m downstream of the obstacle (Fig.2a). The details of geometry and boundary conditions can be found in Tas-Koehler *et al.* (2021). Based on grid independence study performed by Tas-Koehler *et al.* (2021), the computational domain was discretized into 252,000 hexagonal elements (Fig.2b).

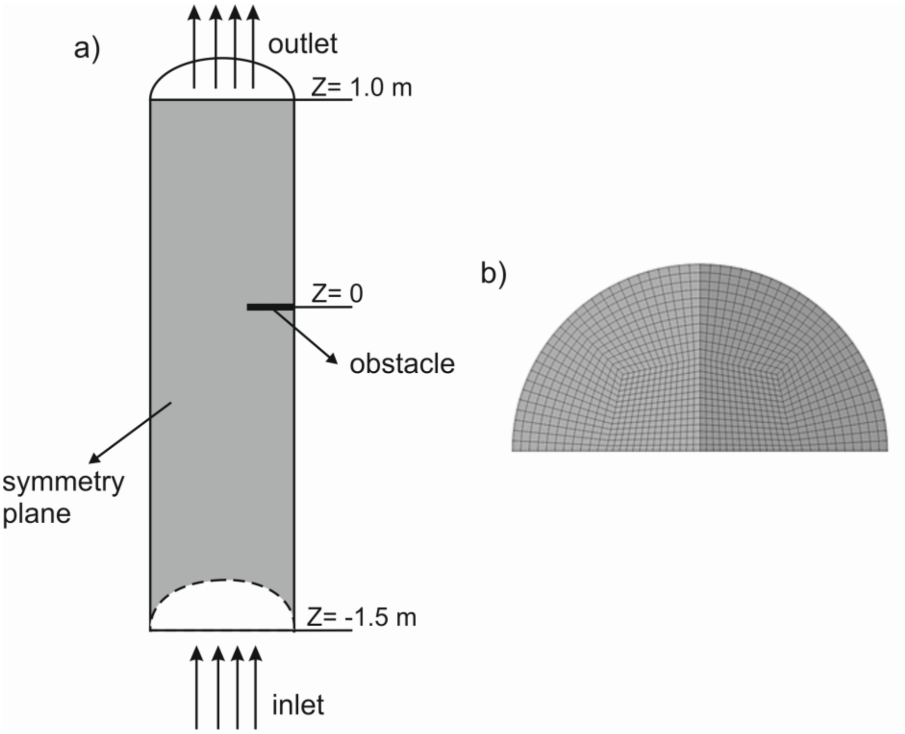

Figure 2: Schematic view of a) geometry and b) mesh (Tas-Koehler et al. (2021)).

In the Eulerian-Eulerian two-fluid model (Yeoh & Tu (2009)) computes the phasic concentration, pressure and velocity fields by solving the continuity equation

$$\frac{\partial(\alpha_k \rho_k)}{\partial t} + \frac{\partial}{\partial x_i}\left(\alpha_k \rho_k \boldsymbol{u}_{i,k}\right) = 0 \tag{5}$$

and the momentum equation

$$\frac{\partial}{\partial t}\left(\alpha_k \rho_k \boldsymbol{u}_{i,k}\right) + \frac{\partial}{\partial x_i}\left(\alpha_k \rho_k \boldsymbol{u}_{i,k} \boldsymbol{u}_{j,k}\right) = -\alpha_k \frac{\partial p_k}{\partial x_i} + \frac{\partial}{\partial x_j}\left[\alpha_k\left(\tau_{ij,k}{}^{Lam} + \tau_{ij,k}{}^{Turb}\right)\right] + \alpha_k \rho_k \boldsymbol{g_i} + \boldsymbol{M}_{i,k}, \tag{6}$$

here for adiabatic conditions. Thereby, k is the phase indicator, α is the volume fraction, ρ is the density, $\boldsymbol{u}_i$ is the velocity component in the i-th direction, p is the pressure, $\tau_{ij}{}^{Lam}$ is the laminar stress tensor, $\tau_{ij}{}^{Turb}$ is the turbulence stress tensor and $\boldsymbol{M}_i$ is the source term in the i-th direction, which includes the interfacial forces i.e. drag force, lift force, wall lubrication force, turbulent dispersion force and virtual mass force. Mathematical expressions for the individual forces are to be found in Tas-Koehler *et al.* (2021). The focus of the current work is on the drag force. All closures for interfacial forces, Bubble-Induced Turbulence (BIT) as well as breakup and coalescence models are summarized in Table 3.

Table 3: Applied models in the simulations.

	Term	Reference
Interfacial force	Drag	Schiller & Naumann (1935)
		Grace *et al.* (1976)

		Ishii & Zuber (1979)
		Bakker & Vandenakker (1994)
		Tomiyama *et al.* (1998)
		Brucato *et al.* (1998)
		Feng & Bolotnov (2016)
		Salibindla *et al.* (2020)
	Lift	Tomiyama *et al.* (2002)
	Turbulent dispersion	Burns *et al.* (2004)
	Wall lubrication	Hosokawa *et al.* (2002)
	Virtual mass	Auton *et al.* (1988), $C_{VM} = 0.5$
Turbulence	Liquid	Shear Stress Transport (SST), Menter (1994)
	BIT	Ma *et al.* (2017)
Population balance model	Coalescence and breakup	MUSIG model, Liao *et al.* (2015)

4. Results

4.1 Performance of existing models

Figure 3 shows the development of cross-section averaged gas fraction in the axial direction of the pipe and different drag coefficient models for the test case 072. Up to $Z = -50$ mm, the Feng model largely and the Ishii&Zuber and Salibindla models slightly underestimate the void fraction, the Bakker, the Grace, the Tomiyama, the Brucato models slightly overestimate the void fraction and the Schiller&Naumann model predicts the void fraction very well compared to experiments. The common point of these models that provide satisfied void fraction estimations i.e. the Ishii&Zuber model, the Bakker model, the Grace model, the Tomiyama model and the Brucato model is that they are based on the same equation (the model of Ishii&Zuber is slightly different)

$$C_D = \left(\frac{24}{Re_b}\left(1 + 0.15{Re_b}^{0.687}\right)\right). \tag{7}$$

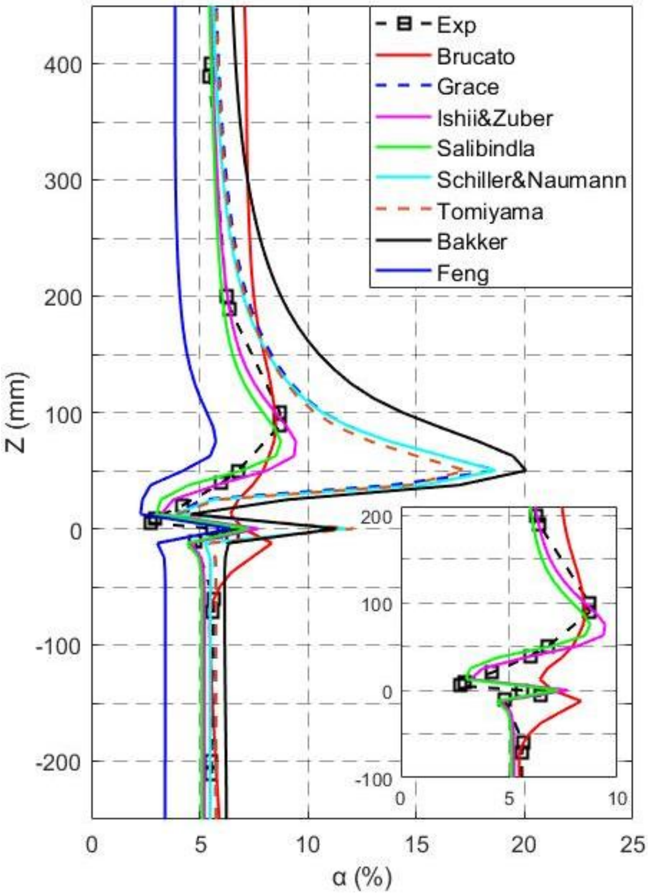

Figure 3: Cross-sectional averaged void fraction along the axial direction for the test 072.

The Bakker model which uses Eq.7, yet, with a different bubble Reynolds number

$$Re_b^* = \frac{\rho_L |\boldsymbol{u}_L - \boldsymbol{u}_G| d_b}{\mu_L + \frac{2}{9}\mu_t} \tag{8}$$

considers the turbulence effect via viscosity. However, it does not improve the results compared to Schiller&Naumann, Grace, Tomiyama, Salibindla and Brucato. It implies that the effect of turbulence is negligible far upstream the obstacle.

For -50 mm $< Z < 0$ mm, the Salibindla and Ishii&Zuber model provides the best void fraction estimations compared to the other models. As shown in Table 1, the Salibindla model takes into account turbulence-induced drag reduction via the Weber number, while the Ishii&Zuber model accounts for elliptical and cap bubble regimes in addition to the spherical one. The findings evidence that as the flow approaches the obstacle, turbulence and bubble deformation plays an increasingly important role. For the obstacle downstream, the Feng model again highly underestimates the void fraction as it does upstream the obstacle. The Bakker model estimates the void fraction between $0 < Z < 100$ mm 2.5 times higher compared to the experiments.

For $0 < Z < 200$ mm, the Tomiyama, the Grace, the Schiller&Naumann and Brucato models overestimate the void fraction. However, the Brucato model predicts void fraction peak around $Z =$ 100 mm well. The Ishii&Zuber and Salibindla models provide the best void fraction prediction here. For 200 mm $< Z <$ 400 mm, the Ishii&Zuber and Salibindla models still predict the void fraction well while the difference between these two and Tomiyama, Grace, Schiller&Naumann models reduces as Z increases. After $Z = 300$ mm, all these five models predict the void fraction well compared to experiments, which is similar to the results in the far-upstream section. The analysis gives evidence that the modelling performance is significantly affected by the obstacle. Nevertheless, for the test case 072 with a superficial liquid velocity of 0.4050 m/s, the Ishii&Zuber and Salibindla is capable of reproducing the average void fraction along the whole flow path, which was also confirmed by the previous study Tas-Koehler *et al.* (2021).

Figure 4 shows the local distribution of void fraction obtained with the different drag models. In line with Figure 3, the Ishii&Zuber, the Salibindla and Brucato models calculate the void fraction distribution well upstream the obstacle. Downstream, the experiment shows a strong gas accumulation (around 16% void fraction) directly behind the obstacle. The Grace, the Schiller&Naumann, the Tomiyama, the Bakker and Feng models predict around 20% higher in this region. For the Ishii&Zuber and Salibindla models, the prediction is better. The Brucato model predicts the distribution of the void fraction well. Yet, it cannot qualitatively capture the high amount of void fraction that is between $0 < Z < 200$ mm.

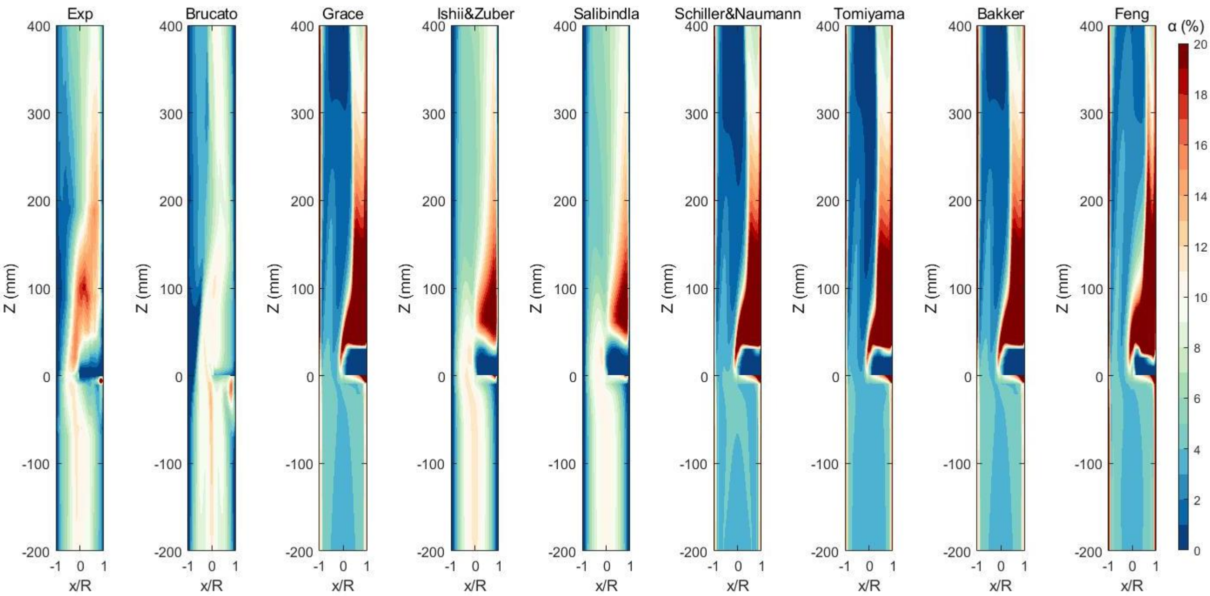

Figure 4: Void fraction for the test 072.

As can be seen from Figures 3 and 4, the Ishii&Zuber and Salibindla models provide similar results, which are satisfying compared to experiments both up- and downstream the obstacle. The Brucato model predicts the upstream well, yet, there is a difference downstream. Although the Brucato model has the capability to capture the location of the void fraction peak that is around $Z = 100$ mm, it overestimates the averaged void fraction near and downstream the obstacle.

Figure 5 shows streamlines of the gas velocity for -200 mm $< Z < 200$ mm. Unlike the Ishii&Zuber and Salibindla, the Brucato model is able to predict a small vortex region upstream that leads to a very small near-wall maximum void fraction region underneath the obstacle. For the obstacle downstream, a vortex region appears after the obstacle. The bubbles are captured by this vortex resulting in a high void fraction here. However, the point is that the shape of the vortex region changes with the drag coefficient model. The Ishii&Zuber model predicts a more remarkable vortex region compared to Salibindla, which causes higher void accumulation. The Brucato model predicts a relatively large vortex region compared to other models. This relatively large vortex region causes a better fit of the void distribution as can be seen in Figure 4.

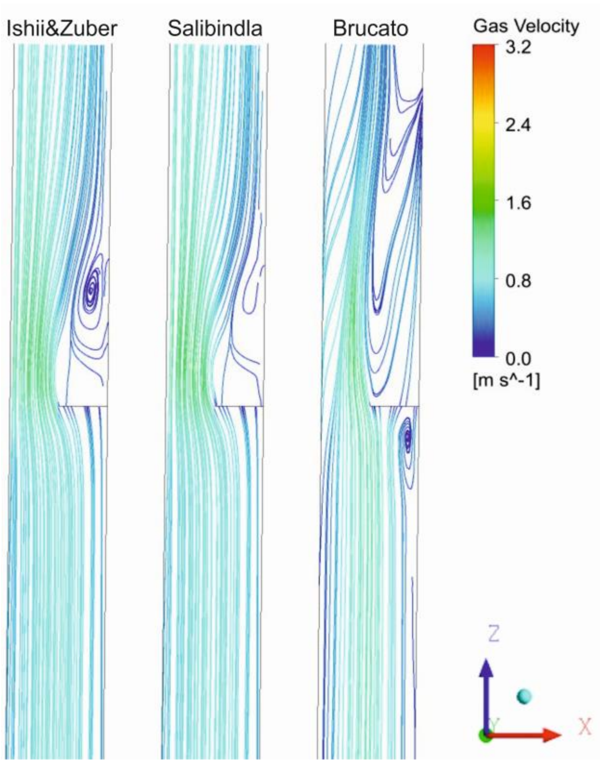

Figure 5: Streamlines for three different drag models: Ishii&Zuber, Salibindla and Brucato for the test 072.

Figure 6 presents the eddy dissipation predictions of Ishii&Zuber, Salibindla and Brucato models. In all three models, the eddy dissipation difference between up- and downstream is obvious: eddy dissipation remarkably increases at downstream the obstacle due to the vortex structure. Referring to Table 1, the common point of the Brucato and Salibindla models is that both models are the modified version of the Tomiyama model (fully contaminated) considering eddy dissipation. While the Tomiyama model overestimates the void fraction in -200 mm $< Z < 200$ mm, the good predictions of the Brucato and Salibindla models show that it is necessary to consider the eddy dissipation impact on the drag model when it exceeds a certain value. According to both models, the drag coefficient may increase with the dissipation rate.

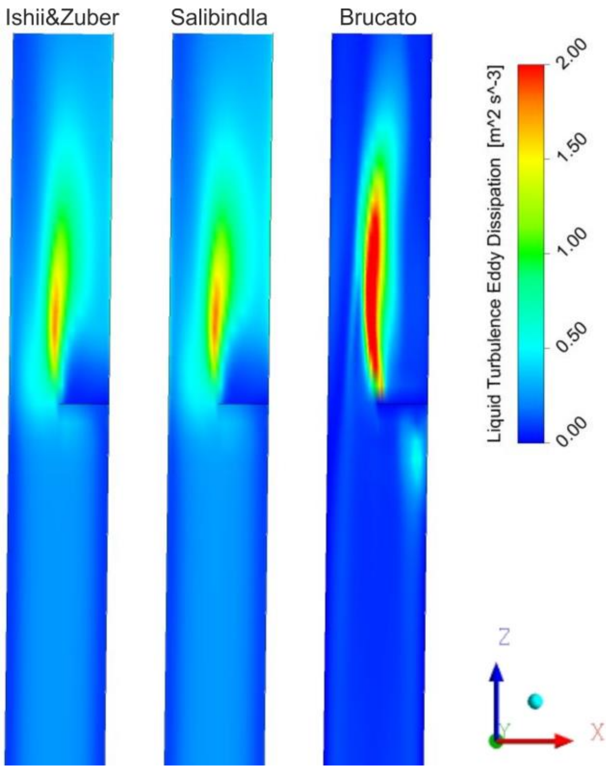

Figure 6: Turbulence eddy dissipation for three different drag models: Ishii&Zuber, Salibindla and Brucato for the test 072.

Now we look at test case 074 with higher liquid velocity. Here, the simulations were very unstable for the Bakker and Feng models. Thus, convergence was not achieved for these two models. Figure 7 shows averaged void fraction along the axial direction. Upstream the obstacle, all the drag models, i.e. Brucato, Grace, Ishii&Zuber, Salibindla, Schiller&Naumann and Tomiyama, slightly underestimate the void fraction compared to experiments, whereby the Brucato model provides the best void prediction. In the region just before the obstacle, the Grace model, the Ishii&Zuber model, the Salibindla model and the Tomiyama model predict the void fraction slightly better. Downstream the obstacle, all the drag models except Brucato highly overestimate the void fraction compared to the experiments. This overestimation can also be seen in Figure 8. Only the Brucato model provides satisfying void fraction results downstream the obstacle. This can be explained with reference to Figure 9. In line with Figure 6, the eddy dissipation increases at downstream the obstacle. However, it also largely increases for test case 074 compared to case 072. Thus, it is even more necessary to consider the impact of turbulence for the drag model.

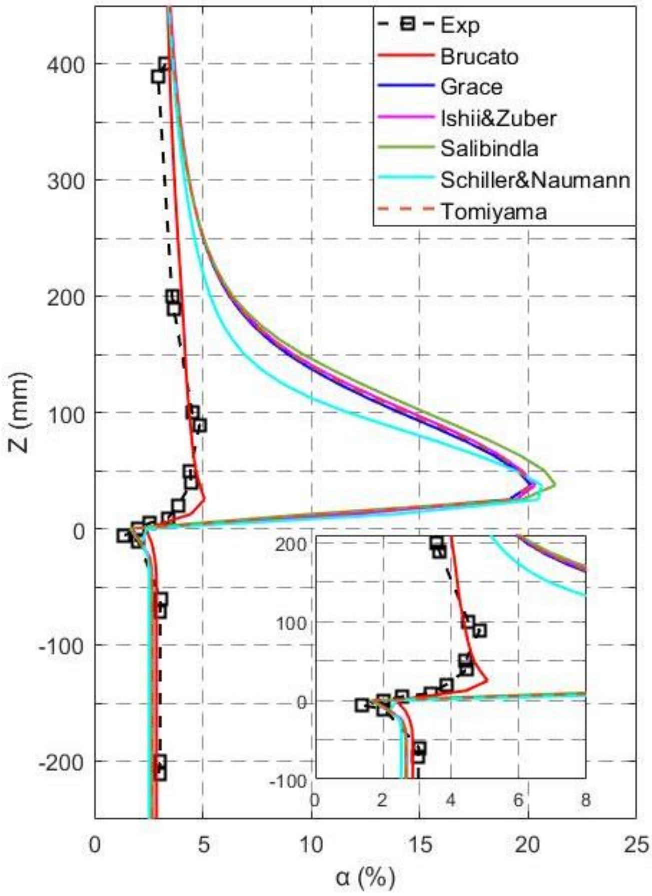

Figure 7: Cross-sectional averaged void fraction along the axial direction for the test 074.

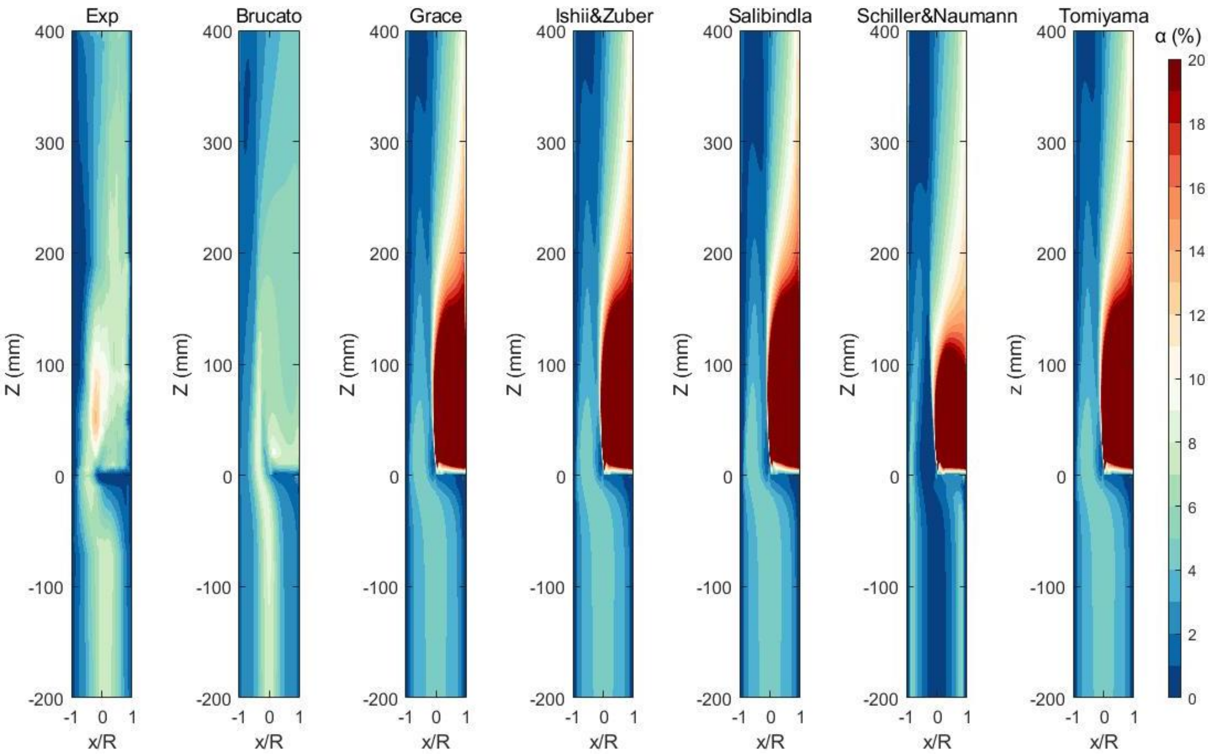

Figure 8: Void fraction for the test 074.

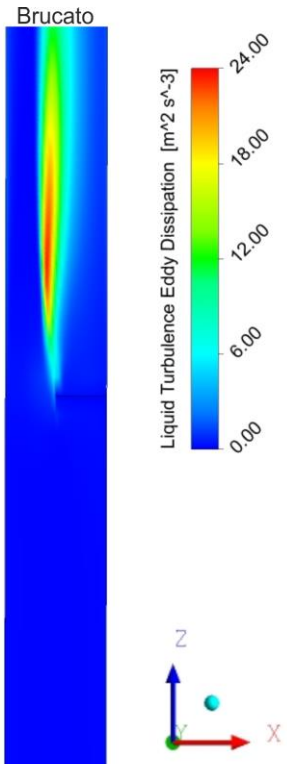

Figure 9: Turbulence eddy dissipation for Brucato model for test 074.

4.2 A hybrid drag model

As a conclusion it can be stated that in the presence of vortex region, i.e. a sudden change of eddy dissipation in the flow field, the Ishii&Zuber model prediction can be improved by taking into account the impact of turbulence effects on the drag model. Thus, a new hybrid model is proposed. According to this hybrid model, the Ishii&Zuber model is used up to a certain eddy dissipation limit ε_L. When the eddy dissipation value exceeds this limit, the simulation switches to the Brucato model. That is

$$C_D = Ishii\&Zuber \;\; \varepsilon < \varepsilon_L \;\; and \;\; Brucato\; else. \tag{9}$$

As a first step, this threshold value was taken as $\varepsilon_L = 1.8\ [m^2 s^{-3}]$ considering on the eddy dissipation distribution that is shown in Figure 6. Figure 10 presents the comparison of the Ishii&Zuber model, the Brucato model and the hybrid model for the test case 072. As shown in the figure, the hybrid model improves the void fraction prediction between around 50 mm $< Z < 200$ mm where relatively high eddy dissipation compared to upstream is observed. After the hybrid model was found to improve the simulations, different threshold values were simulated to obtain the best agreement with the measurements. Figure 11 presents the void fraction profiles for selected different threshold values i.e. $\varepsilon_L = 0.5$, $\varepsilon = 1.0$, $\varepsilon_L = 1.5$, $\varepsilon_L = 1.8$ and $\varepsilon_L = 2.0\ [m^2 s^{-3}]$. Upstream the obstacle, all the threshold values provide the same void fraction predictions since the eddy dissipation value is very low. Downstream the obstacle, the threshold value that best matches the experiments is the $\varepsilon_L = 1.5\ [m^2 s^{-3}]$. Thus, $\varepsilon_L = 1.5\ [m^2 s^{-3}]$ was used for the rest of the study.

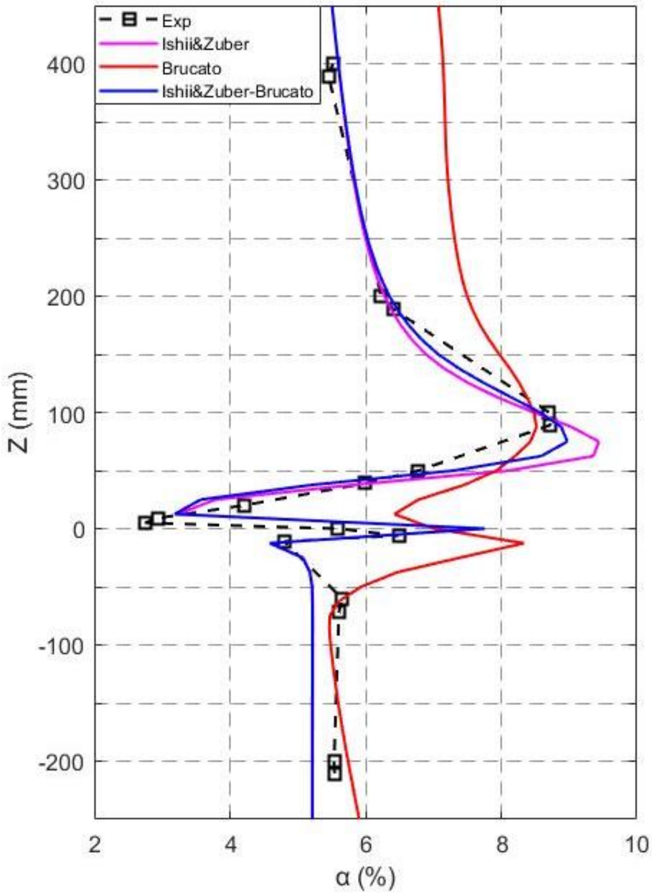

Figure 10: Comparison of cross-sectional averaged void fraction along the axial direction for Ishii&Zuber, Brucato and hybrid model for the test 072.

Figure 12 shows radial void distributions for Ishii&Zuber, Brucato and the hybrid model at different cross-sections for the test case 072. For $Z = -200$ mm, the Brucato model gives a slightly different void prediction compared to Ishii&Zuber and hybrid model, which provide the same results. For $Z = -11$ mm (just before the obstacle), Brucato underestimates and overestimates the void fraction for the right and left side of the pipe respectively whereas Ishii&Zuber and hybrid models predict well. For $Z = 50$ mm (where the vortex structure starts to occur), Ishii&Zuber and hybrid models slightly overestimate the void fraction up to $X = -10$ mm while the Brucato model slightly underestimates it. The hybrid model improves the void fraction prediction between $-10\text{ mm} < X < 2\text{ mm}$. After X= 2 mm, Ishii&Zuber and hybrid models provide different void estimations, which are unsatisfactory. The Brucato model generally underestimates the void fraction except in the area $-5\text{ mm} < X < -10\text{ mm}$. For $Z = 100$ mm, $Z = 200$ mm and $Z = 400$ mm, the Ishii&Zuber and hybrid models predict approximately the same void fraction, and the Brucato model does not provide better results than these two models.

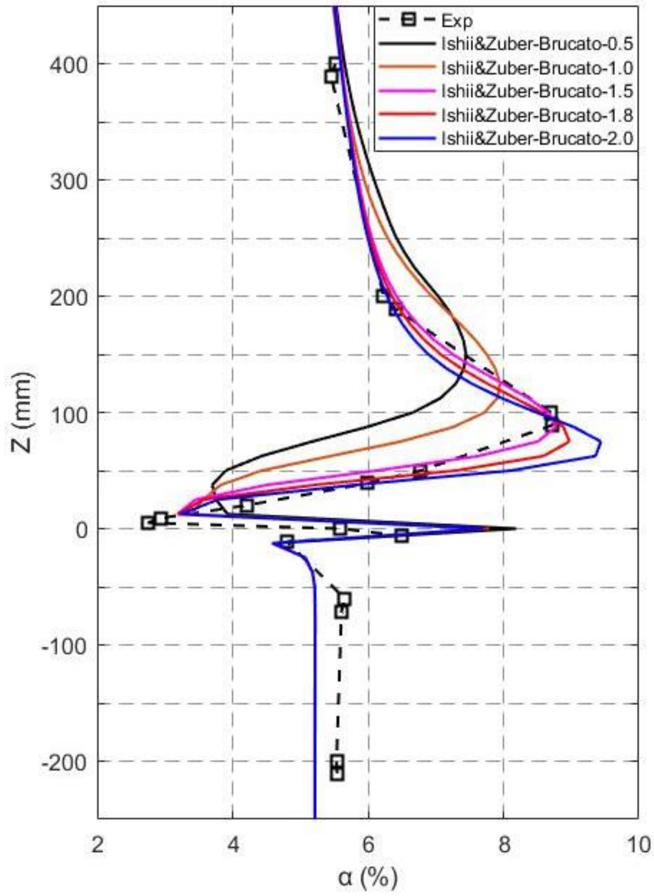

Figure 11: Comparison of cross-sectional averaged void fraction for different eddy dissipation limits for the test 072.

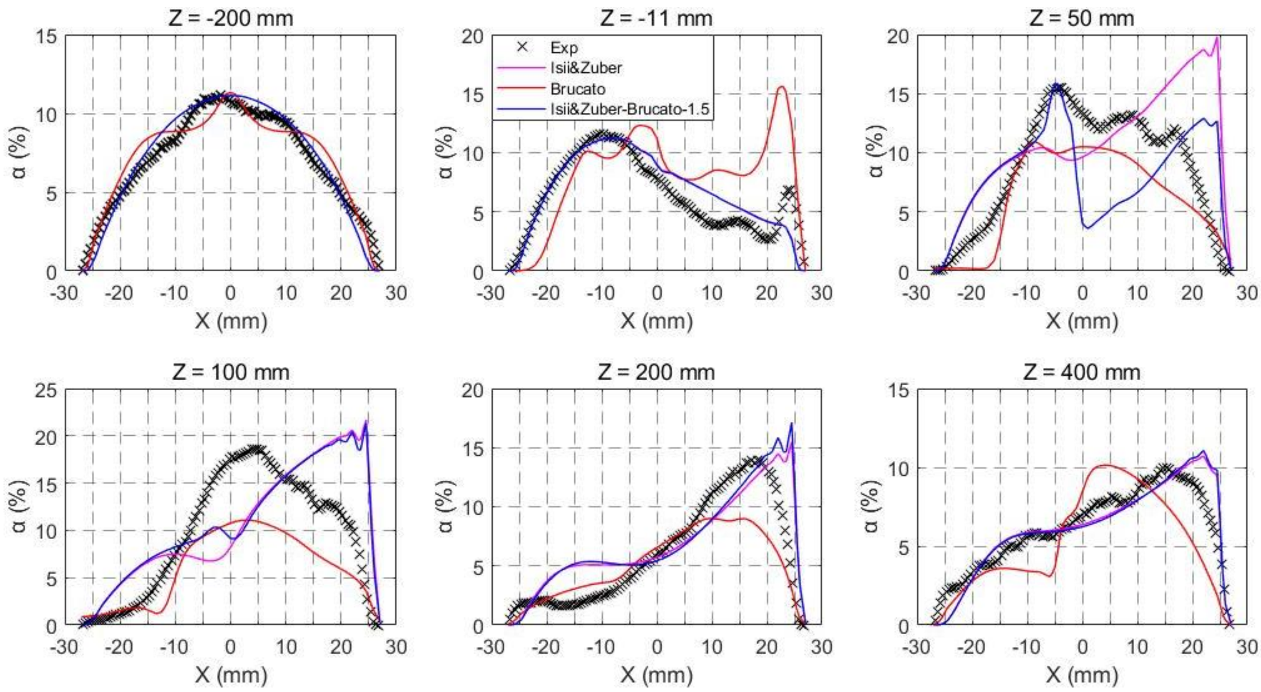

Figure 12: Radial void fraction distribution for Ishii&Zuber, Brucato and hybrid model for different axial positions for the test 072.

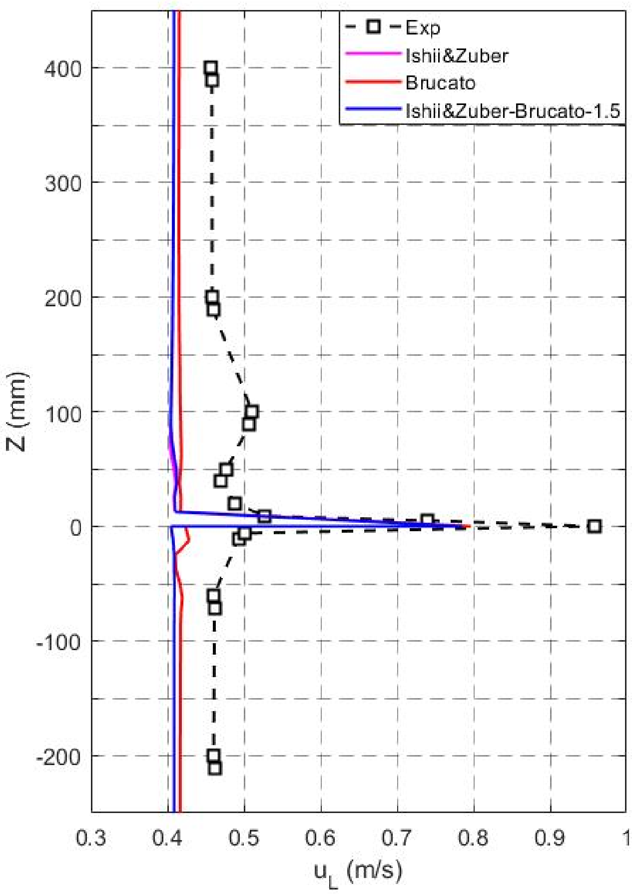

Figure 13: Cross-sectional averaged liquid velocity for the test 072.

Figure 13 shows the averaged liquid velocity along the axial direction for the test case 072. As can be seen from the figure, all the drag models underestimate the velocity compared to the experiments at all Z positions. The Brucato model provides a slightly better liquid velocity prediction. Yet, the difference is very small. The averaged axial gas velocity is shown in Figure 14. The Ishii&Zuber and hybrid models predict the gas velocity better than the Brucato model.

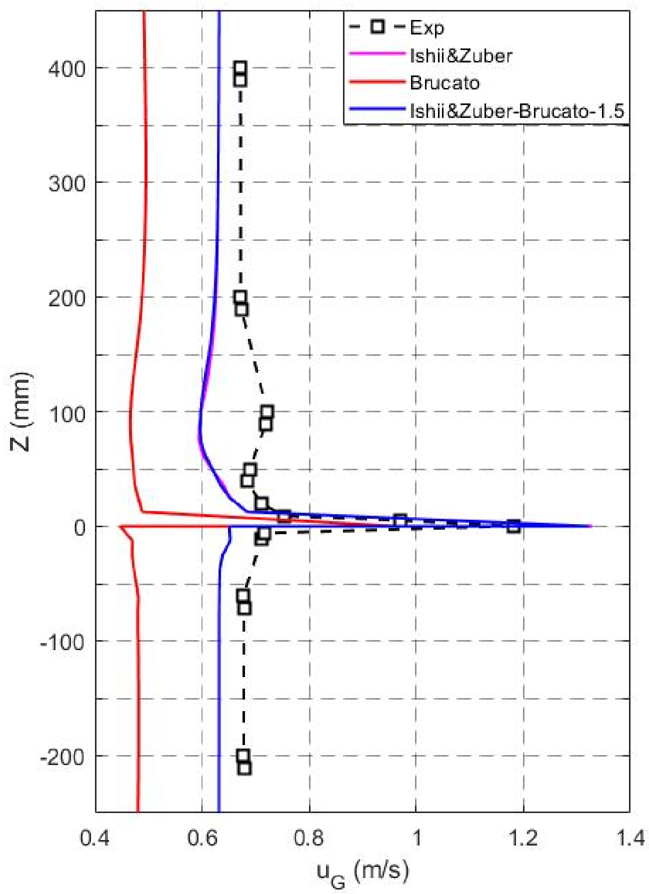

Figure 14: Cross-sectional averaged gas velocity for the test 072.

Considering the test case 074, Figure 15 shows the comparison of averaged void fraction for the Brucato and hybrid models. Although the Brucato model predicts the void fraction except in $-50\ \text{mm} < X < 150\ \text{mm}$ slightly better compared to the hybrid model, the hybrid model improves the prediction compared to Brucato in this region.

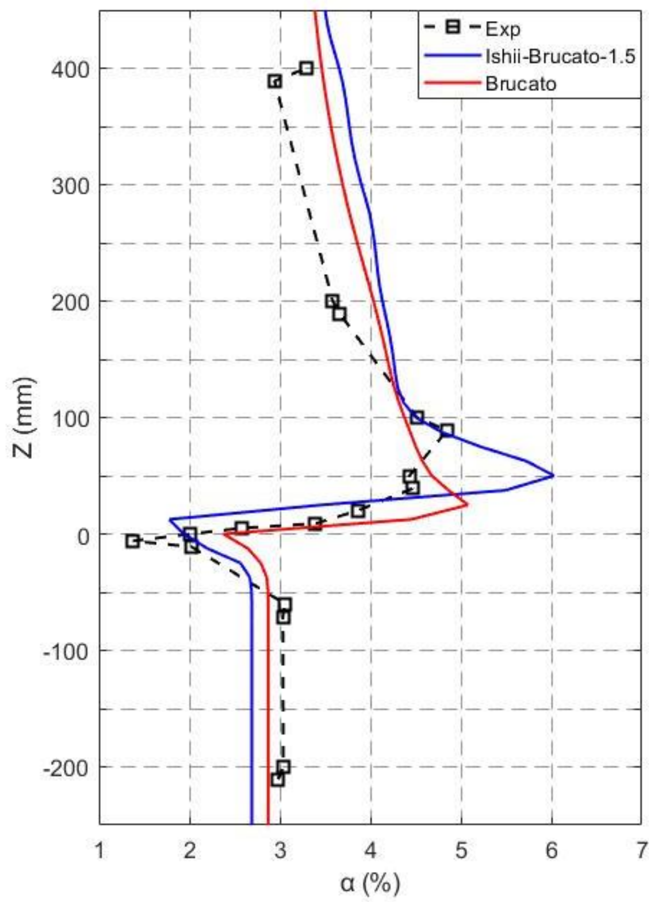

Figure 15: Comparison of cross-sectional averaged void fraction along the axial direction for Ishii&Zuber, Brucato and hybrid model for test 074.

The radial void distribution for the Brucato and hybrid model is shown in Figure 16. For $Z = -200$ mm, the Brucato model predicts the void fraction well except in 5 mm $< X < 20$ mm while the hybrid model predicts well near the wall. For $Z = -11$ mm, the Brucato model generally predicts the void distribution better. For $Z = 50$ mm, the Brucato model estimations agree better with the experiments here while the hybrid model largely overestimates the void fraction on the right hand side of the pipe. For $Z = 100$ mm, the hybrid model provides a better prediction between $0 < X < 20$ mm whereas the Brucato model provides a better prediction between -20 mm $< X < -5$ mm. For $Z = 200$ mm and $Z = 400$ mm, the hybrid and Brucato models provide similar void fraction distributions. For $Z = 200$ mm, they overestimate the void fraction between -27 mm $< X < 0$ whereas they underestimate it between $0 < X < 20$ mm. For $Z = 400$ mm, they underestimate the void fraction between -20 mm $< X < 20$ mm (except between -10 mm $< X < 0$ for the hybrid model).

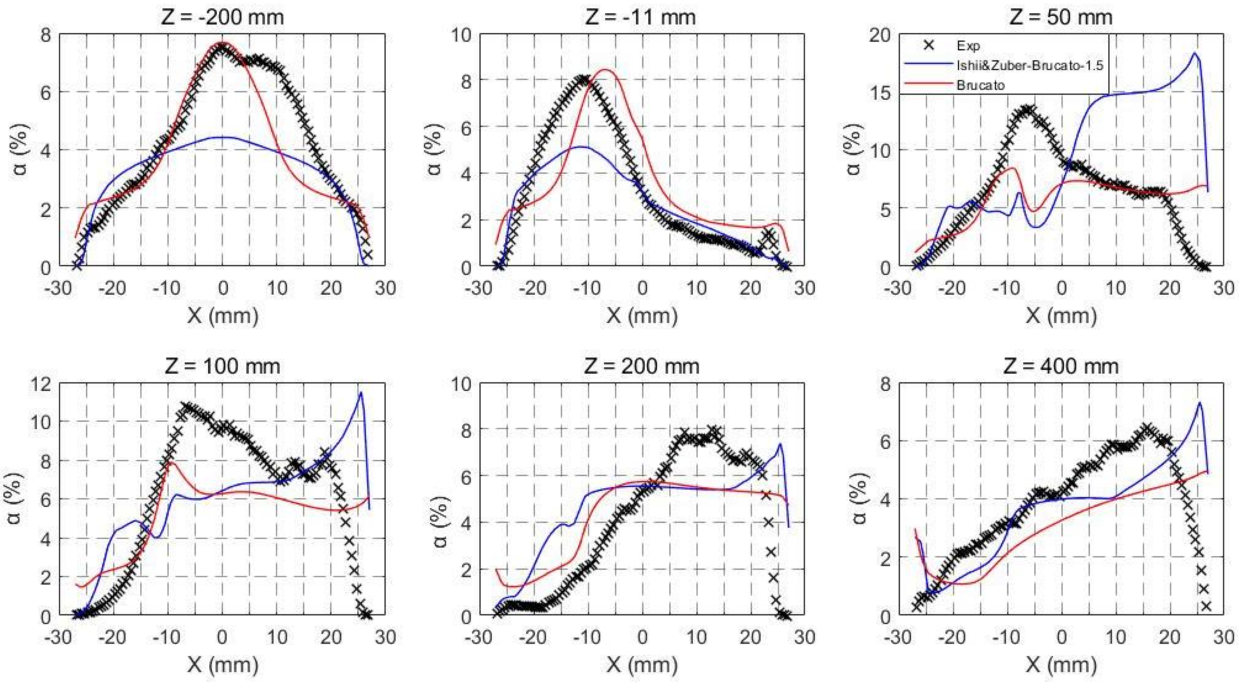

Figure 16: Radial void fraction distribution for Brucato and hybrid model for different axial positions for the test 074.

Figure 17 and 18 show the averaged liquid and gas velocities for the test 074 respectively. As it can be seen in Figure 17, all models provide approximately the same liquid velocity prediction. Whereas the prediction agrees well with the experiments at downstream the obstacle, it is underestimated up to $Z = 200$ mm. The liquid velocity changes in the vortex region cannot be accurately estimated independent of the drag model by simulations. As shown in Figure 18, the hybrid model predicts the gas velocity well compared to the experiments downstream the obstacle. However, the Brucato model moderately underestimates it here. As for the liquid velocity, both models cannot capture the velocity changes at the obstacle downstream adequately.

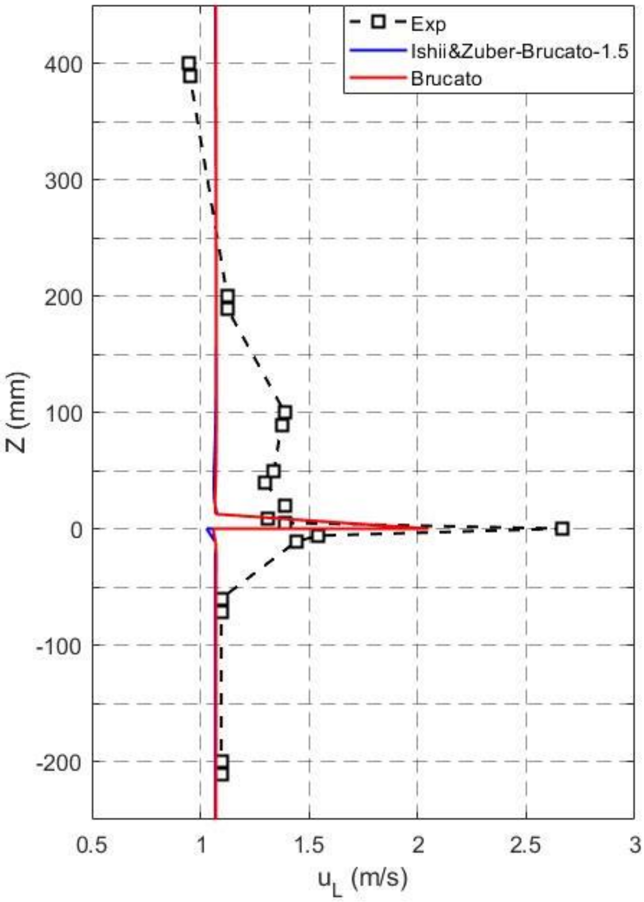

Figure 17: Cross-sectional averaged liquid velocity for the test 074.

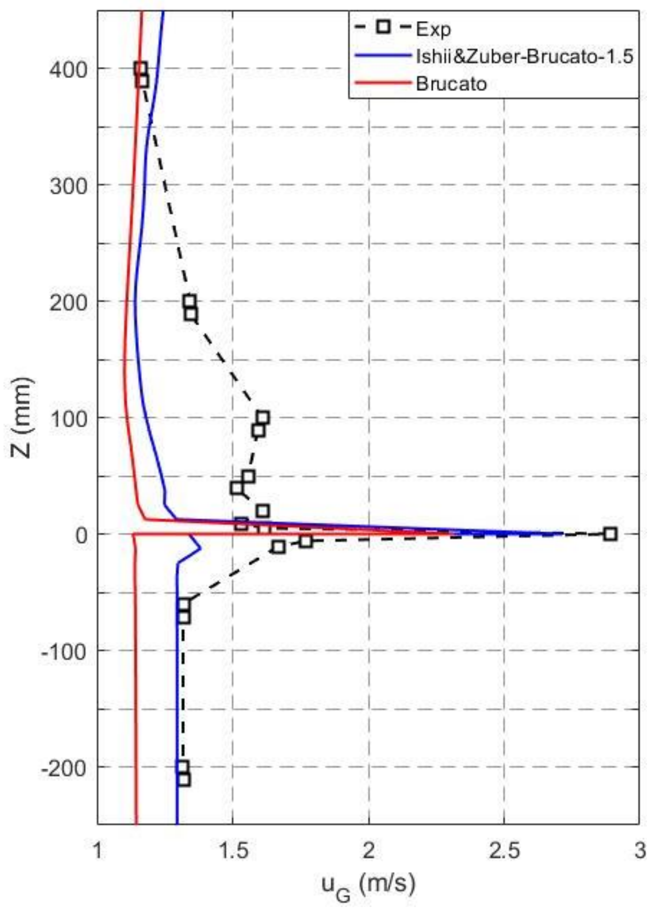

Figure 18: Cross-sectional averaged gas velocity for the test 074.

5. Conclusions

In this study, we examined the capability of different drag models for disperse gas-liquid flow at two different turbulence conditions for the case of an obstacle in a pipe that produces a pronounced vortex region. The Feng model underestimates the void fraction compared to the experiments for the low-velocity case for both the upstream (lower turbulence) and downstream (higher turbulence-vortex) region of the obstacle. This is attributed to the fact that this model is purely based on the Tomiyama model which holds for pure liquid (without contamination) systems. In addition, the simulations with the Feng model for the high-velocity case were highly unstable and no results could be obtained. The Bakker model moderately overestimates the void fraction compared to the experiments upstream of the obstacle for the low-velocity case. However, it extremely overestimates the void fraction downstream of the obstacle, especially in the vortex region. One reason may be that the bubble Reynolds number in the Bakker model has been formulated differently than other models. The coefficient used for the turbulent viscosity may not be applicable in the case of high turbulence.

For the low-velocity and high-velocity cases, the Grace model, the Tomiyama model, the Ishii&Zuber model, the Schiller&Naumann model, the Salibindla model and the Brucato model predict the void fraction well. It is attributed to the fact that neither turbulence nor bubble deformation are significant here. Thus, these models provide good void fraction predictions independent of whether or not the turbulence and/or bubble deformation effects are taken into account. However, the difference between low- and high-velocity cases appears downstream of the obstacle in the vortex region. For the low-velocity case, the Schiller&Naumann model, the Tomiyama model and the Grace model highly overestimate the void fraction. The Ishii&Zuber model, which uses a slightly different definition compared to Eq. 7 and the Salibindla model that includes a turbulence eddy dissipation correction, provide the best void prediction here. Yet, the Brucato model is the only model that captures the void peak. For the high-velocity case, all the models largely overestimate the void fraction, except the Brucato model. Based on these findings, we concluded that in the presence of a vortex region with high eddy dissipation changes, the drag model that considers the only bubble deformation is not sufficient. Furthermore, the turbulence effect should be accounted for when the eddy dissipation exceeds a limit value of ($\varepsilon_L = 1.5\ \mathrm{m^2\ s^{-3}}$). Consequently, we propose a hybrid drag model depending on the eddy dissipation limit, which improves the void fraction prediction.

We found that liquid and gas velocities are generally underpredicted for the low-velocity case compared to the experimental data. However, the Brucato model provides less accurate gas velocity prediction compared to the Ishii&Zuber and hybrid models. For the high-velocity case, where the Brucato and hybrid models provide similar liquid velocity estimations upstream, the hybrid model predicts better the gas velocity. Both models generally underestimate the gas and liquid velocities downstream.

As consequence, the influence of turbulence on the bubbles through the drag coefficient closure improved the void fraction predictions, especially for high turbulent flow. Thus, it can be concluded that the effects of turbulent eddies on drag force are needed to be considered for CFD modelling. Another point is that it is still necessary to improve the gas and liquid velocity predictions, especially for downstream. The explanation of gas and liquid velocity underestimation may be due to insufficient turbulence modelling. Instead of using a two-equation model, using an advanced turbulence model like the Reynolds Stress Model may improve the velocity predictions in the vortex region.

References

Asad, A., Kratzsch, C., & Schwarze, R. (2017). Influence of drag closures and inlet conditions on bubble dynamics and flow behavior inside a bubble column. *Engineering Applications of Computational Fluid Mechanics, 11*(1), 127-141. Retrieved from <Go to ISI>://WOS:000388586200005. doi:10.1080/19942060.2016.1249410

Auton, T. R., Hunt, J. C. R., & Prudhomme, M. (1988). The Force Exerted on a Body in Inviscid Unsteady Non-Uniform Rotational Flow. *Journal of Fluid Mechanics, 197*, 241-257. doi:10.1017/S0022112088003246

Bakker, A., & Vandenakker, H. E. A. (1994). A Computational Model for the Gas-Liquid Flow in Stirred Reactors. *Chemical Engineering Research & Design, 72*(A4), 594-606. Retrieved from <Go to ISI>://WOS:A1994PE66500013.

Besagni, G., Guedon, G. R., & Inzoli, F. (2018). Computational fluid-dynamic modeling of the mono-dispersed homogeneous flow regime in bubble columns. *Nuclear Engineering and Design, 331*, 222-237. doi:10.1016/j.nucengdes.2018.03.003

Brucato, A., Grisafi, F., & Montante, G. (1998). Particle drag coefficients in turbulent fluids. *Chemical Engineering Science, 53*(18), 3295-3314. Retrieved from <Go to ISI>://WOS:000076195300009. doi:Doi 10.1016/S0009-2509(98)00114-6

Burns, A. D., Frank, T., Hamill, I., & Shi, J.-M. (2004). *The Favre averaged drag model for turbulent dispersion in Eulerian multi-phase flows*. Paper presented at the 5th Iinternational Conference on Multiphase Flow, ICMF, Yokohama, Japan.

Chen, P. (2004). *Modeling the fluid dynamics of bubble column flows.* (Ph.D. Thesis), Sever Institute of Washington University,

Doroodchi, E., Evans, G. M., Schwarz, M. P., Lane, G. L., Shah, N., & Nguyen, A. (2008). Influence of turbulence intensity on particle drag coefficients. *Chemical Engineering Journal, 135*(1-2), 129-134. Retrieved from <Go to ISI>://WOS:000251593300018. doi:10.1016/j.cej.2007.03.026

Feng, J., & Bolotnov, I. (2016). *Single bubble drag force evaluation in turbulent flow based on DNS result.* Paper presented at the ANS Winter Meeting, Las Vegas, NV.

Grace, J. R., Wairegi, T., & Nguyen, T. H. (1976). Shapes and Velocities of Single Drops and Bubbles Moving Freely through Immiscible Liquids. *Transactions of the Institution of Chemical Engineers, 54*(3), 167-173. Retrieved from <Go to ISI>://WOS:A1976CD39200004.

Guan, X. P., Li, X. J., Yang, N., & Liu, M. Y. (2020). CFD simulation of gas-liquid flow in stirred tanks: Effect of drag models. *Chemical Engineering Journal, 386*. Retrieved from <Go to ISI>://WOS:000551293900003. doi:ARTN 121554

10.1016/j.cej.2019.04.134

Gupta, A., & Roy, S. (2013). Euler-Euler simulation of bubbly flow in a rectangular bubble column: Experimental validation with Radioactive Particle Tracking. *Chemical Engineering Journal, 225*, 818-836. Retrieved from <Go to ISI>://WOS:000321313800094. doi:10.1016/j.cej.2012.11.012

Hosokawa, S., Tomiyama, A., Misaki, S., & Hamada, T. (2002). *Lateral migration of single bubbles due to the presence of wall*. Paper presented at the Proceedings of the ASME Joint U.S.-European Fluids Engineering Division Conference, FEDSM2002, Montreal, Canada.

Ishii, M., & Zuber, N. (1979). Drag Coefficient and Relative Velocity in Bubbly, Droplet or Particulate Flows. *Aiche Journal, 25*(5), 843-855. Retrieved from <Go to ISI>://WOS:A1979HN38300012. doi:DOI 10.1002/aic.690250513

Jiang, X. D., Yang, N., & Yang, B. L. (2016). Computational fluid dynamics simulation of hydrodynamics in the riser of an external loop airlift reactor. *Particuology, 27*, 95-101. Retrieved from <Go to ISI>://WOS:000378959000011. doi:10.1016/j.partic.2015.05.011

Jin, D., Xiong, J. B., & Cheng, X. (2019). Investigation on interphase force modeling for vertical and inclined upward adiabatic bubbly flow. *Nuclear Engineering and Design, 350*, 43-57. doi:10.1016/j.nucengdes.2019.05.005

Karimi, M., Akdogan, G., Dellimore, K. H., & Bradshaw, S. M. (2012). *Comparion of different drag coefficient correlations in the CFD modelling of a laboratory-scale Rushton-turbine flotation tank*. Paper presented at the NInth International Conference on CFD in the Minerals and Process Industries, CSIRO, Melbourne, Australia.

Khopkar, A. R., & Ranade, V. V. (2006). CFD simulation of gas-liquid stirred vessel: VC, S33, and L33 flow regimes. *Aiche Journal, 52*(5), 1654-1672. Retrieved from <Go to ISI>://WOS:000237128700003. doi:10.1002/aic.10762

Lane, G. L., Schwarz, M. P., & Evans, G. M. (2002). Predicting gas-liquid flow in a mechanically stirred tank. *Applied Mathematical Modelling, 26*(2), 223-235. Retrieved from <Go to ISI>://WOS:000174309600009. doi:Pii S0307-904x(01)00057-9

Doi 10.1016/S0307-904x(01)00057-9

Lane, G. L., Schwarz, M. P., & Evans, G. M. (2005). Numerical modelling of gas-liquid flow in stirred tanks. *Chemical Engineering Science, 60*(8-9), 2203-2214. Retrieved from <Go to ISI>://WOS:000227864000010. doi:10.1016/j.ces.2004.11.046

Liao, Y. X., Ma, T., Liu, L., Ziegenhein, T., Krepper, E., & Lucas, D. (2018). Eulerian modelling of turbulent bubbly flow based on a baseline closure concept. *Nuclear Engineering and Design, 337*, 450-459. doi:10.1016/j.nucengdes.2018.07.021

Liao, Y. X., Rzehak, R., Lucas, D., & Krepper, E. (2015). Baseline closure model for dispersed bubbly flow: Bubble coalescence and breakup. *Chemical Engineering Science, 122*, 336-349. doi:10.1016/j.ces.2014.09.042

Ma, T., Santarelli, C., Ziegenhein, T., Lucas, D., & Frohlich, J. (2017). Direct numerical simulation-based Reynolds-averaged closure for bubble-induced turbulence. *Physical Review Fluids, 2*(3). doi:10.1103/PhysRevFluids.2.034301

Masood, R. M. A., & Delgado, A. (2014). Numerical investigation of the interphase forces and turbulence closure in 3D square bubble columns. *Chemical Engineering Science, 108*, 154-168. Retrieved from <Go to ISI>://WOS:000332392100015. doi:10.1016/j.ces.2014.01.004

Menter, F. R. (1994). 2-Equation Eddy-Viscosity Turbulence Models for Engineering Applications. *Aiaa Journal, 32*(8), 1598-1605. doi:10.2514/3.12149

Morsi, S. A., & Alexander, A. J. (1972). Investigation of Particle Trajectories in 2-Phase Flow Systems. *Journal of Fluid Mechanics, 55*(Sep26), 193-+. Retrieved from <Go to ISI>://WOS:A1972N745700001. doi:Doi 10.1017/S0022112072001806

Neumann-Kipping, M., Bieberle, A., & Hampel, U. (2020). Investigations on bubbly two-phase flow in a constricted vertical pipe. *International Journal of Multiphase Flow, 130*. doi:10.1016/j.ijmultiphaseflow.2020.103340

Pourtousi, M., Sahu, J. N., & Ganesan, P. (2014). Effect of interfacial forces and turbulence models on predicting flow pattern inside the bubble column. *Chemical Engineering and Processing-Process Intensification, 75,* 38-47. Retrieved from <Go to ISI>://WOS:000331924000005. doi:10.1016/j.cep.2013.11.001

Salibindla, A. K. R., Masuk, A. U. M., Tan, S. Y., & Ni, R. (2020). Lift and drag coefficients of deformable bubbles in intense turbulence determined from bubble rise velocity. *Journal of Fluid Mechanics, 894*. Retrieved from <Go to ISI>://WOS:000530307300001. doi:ARTN A20

10.1017/jfm.2020.244

Schiller, L., & Naumann, A. (1935). A drag coefficient correlation. *Z. Ver. Deutsch. Ing. 77,* 318-320.

Silva, M. K., d'Avila, M. A., & Mori, M. (2012). Study of the interfacial forces and turbulence models in a bubble column. *Computers & Chemical Engineering, 44,* 34-44. Retrieved from <Go to ISI>://WOS:000306603600004. doi:10.1016/j.compchemeng.2012.04.007

Simonnet, M., Gentric, C., Olmos, E., & Midoux, N. (2007). Experimental determination of the drag coefficient in a swarm of bubbles. *Chemical Engineering Science, 62*(3), 858-866. Retrieved from <Go to ISI>://WOS:000243714900019. doi:10.1016/j.ces.2006.10.012

Tabib, M. V., Roy, S. A., & Joshi, J. B. (2008). CFD simulation of bubble column - An analysis of interphase forces and turbulence models. *Chemical Engineering Journal, 139*(3), 589-614. Retrieved from <Go to ISI>://WOS:000256652500019. doi:10.1016/j.cej.2007.09.015

Tas-Koehler, S., Lecrivain, G., Krepper, E., Unger, S., & Hampel, U. (2020). Numerical investigation on the effect of transversal fluid field deformation on heat transfer in a rod bundle with mixing vanes. *Nuclear Engineering and Design, 361*. doi:10.1016/j.nucengdes.2020.110575

Tas-Koehler, S., Neumann-Kipping, M., Liao, Y. X., Krepper, E., & Hampel, U. (2021). CFD simulation of bubbly flow around an obstacle in a vertical pipe with a focus on breakup and coalescence modelling. *International Journal of Multiphase Flow*. doi:doi.org/10.1016/j.ijmultiphaseflow.2020.103528

Tomiyama, A., Kataoka, I., Zun, I., & Sakaguchi, T. (1998). Drag coefficients of single bubbles under normal and micro gravity conditions. *Jsme International Journal Series B-Fluids and Thermal Engineering, 41*(2), 472-479. doi:10.1299/jsmeb.41.472

Tomiyama, A., Tamai, H., Zun, I., & Hosokawa, S. (2002). Transverse migration of single bubbles in simple shear flows. *Chemical Engineering Science, 57*(11), 1849-1858. doi:10.1016/S0009-2509(02)00085-4

Wang, Q. G., & Yao, W. (2016). Computation and validation of the interphase force models for bubbly flow. *International Journal of Heat and Mass Transfer, 98,* 799-813. Retrieved from <Go to ISI>://WOS:000375360600075. doi:10.1016/j.ijheatmasstransfer.2016.03.064

Yamoah, S., Martinez-Cuenca, R., Monros, G., Chiva, S., & Macian-Juan, R. (2015). Numerical investigation of models for drag, lift, wall lubrication and turbulent dispersion forces for the simulation of gas-liquid two-phase flow. *Chemical Engineering Research & Design, 98,* 17-35. Retrieved from <Go to ISI>://WOS:000356755500002. doi:10.1016/j.cherd.2015.04.007

Yeoh, G. H., & Tu, J. Y. (2009). *Computational Techniques for Multiphase Flows*: Butterworth-Heinemann.

Zhang, D., Deen, N. G., & Kuipers, J. A. M. (2006). Numerical simulation of the dynamic flow behavior in a bubble column: A study of closures for turbulence and interface forces. *Chemical Engineering Science, 61*(23), 7593-7608. Retrieved from <Go to ISI>://WOS:000242486500003. doi:10.1016/j.ces.2006.08.053

Zhang, D. Z., & VanderHeyden, W. B. (2002). The effects of mesoscale structures on the macroscopic momentum equations for two-phase flows. *International Journal of Multiphase Flow, 28*(5), 805-822. Retrieved from <Go to ISI>://WOS:000175820800006. doi:Pii S0301-9322(02)00005-8

Doi 10.1016/S0301-9322(02)00005-8

Declaration of Interest Statement

02.04.2021

Dear Editor,

The authors certify that they have no affiliations or involvement in any organization or entity with any financial interest or non-financial interest in the subject matter or materials discussed in this manuscript.

We confirm that this work is original and has not been published elsewhere, nor is it currently under consideration for publication elsewhere.

Sincerely,

Sibel Tas-Koehler